Bone Reports 16 (2022) 101172

Contents lists available at ScienceDirect

Bone Reports

journal homepage: www.elsevier.com/locate/bonr

Contemporary kidney transplantation has a limited impact on bone microarchitecture

Catarina Meng [a,b], Hanne Skou Jørgensen [a,c], Lieve Verlinden [d], Nathalie Bravenboer [e], Henriette de Loor [a], Patrick C. D'Haese [f], Geert Carmeliet [d], Pieter Evenepoel [a,g,*]

[a] Department of Microbiology, Immunology and Transplantation, Nephrology and Renal Transplantation Research Group, KU Leuven, Leuven, Belgium
[b] Faculty of Medicine, University of Porto, Porto, Portugal
[c] Department of Kidney Diseases, Aarhus University Hospital, Aarhus, Denmark
[d] Department of Chronic Diseases and Metabolism, Laboratory of Clinical and Experiment Endocrinology, KU Leuven, Leuven, Belgium
[e] Department of Clinical Chemistry, Amsterdam University Medical Center, Vrije Universiteit, Amsterdam Movement Sciences, Amsterdam, the Netherlands
[f] Laboratory of Pathophysiology, University of Antwerp, Wilrijk, Belgium
[g] Department of Nephrology and Renal Transplantation, University Hospitals Leuven, Leuven, Belgium

ARTICLE INFO

Keywords:
Bone density
Bone histomorphometry
Kidney transplantation
Chronic kidney disease – mineral and bone disorder
Osteoporosis
X-Ray Microtomography

ABSTRACT

Bone microarchitecture is an important component of bone quality and disturbances may reduce bone strength and resistance to trauma. Kidney transplant recipients have an excess risk of fractures, and bone loss affecting both trabecular and cortical bone compartments have been demonstrated after kidney transplantation. The primary aim of this study was to investigate the impact of kidney transplantation on trabecular and cortical bone microarchitecture, assessed by histomorphometry and micro computed tomography (μCT). Iliac crest bone biopsies, analyzed by bone histomorphometry and μCT, were performed at time of kidney transplantation and 12 months post-transplantation in an unselected cohort of 30 patients. Biochemical markers of mineral metabolism and bone turnover were measured at both time-points. At 12 months post-transplantation, bone turnover was low in 5 (17%) and normal in 25 (83%) patients. By histomorphometry, bone remodeling normalized, with decreases in eroded perimeters (4.0 to 2.1%, $p = 0.02$) and number of patients with marrow fibrosis (41 to 0%, $p < 0.001$). By μCT, trabecular thickness (134 to 125 μM, $p = 0.003$) decreased slightly. Other parameters of bone volume and microarchitecture, including cortical thickness (729 to 713 μm, $p = 0.73$) and porosity (10.2 to 9.5%, $p = 0.15$), remained stable. We conclude that kidney transplantation with current immunosuppressive protocols has a limited impact on bone microarchitecture.

1. Introduction

Kidney transplant recipients experience an excessively high fracture risk, especially during the first year after transplantation, with risks exceeding what is seen in the dialysis population by 30% (Ball et al. 2002). Immunosuppressive drugs, particularly steroids, and persistent hyperparathyroidism play a role in post-transplantation bone disease, along with *de novo* abnormalities related to poor kidney graft function and age-related changes (Bouquegneau et al., 2016).

Areal bone mineral density (BMD) by dual-energy x-ray absorptiometry (DXA) is the most common assessment when monitoring bone quantity. Historical cohort studies reported BMD losses exceeding 10% during the first year after kidney transplantation (Julian et al., 1991; Heaf, 2003). More recent studies show less pronounced bone loss, perhaps paralleling the increased use of steroid minimization protocols (Iyer et al., 2014; Evenepoel et al., 2020; Evenepoel et al., 2017). While predicting fractures in *de novo* kidney transplant recipients (Evenepoel et al., 2019) a low BMD does not fully explain the risk. This is not remarkable, as DXA cannot inform on bone *quality*; bone mineralization, turnover, and microarchitecture are all characteristics affecting bone

Abbreviations: 2D, two-dimensional; 3D, three-dimensional; BMD, bone mineral density; BALP, bone-specific alkaline phosphatase; CKD, chronic kidney disease; DXA, dual-energy x-ray absorptiometry; eGFR, estimated glomerular filtration rate; HRpQCT, high-resolution peripheral quantitative computed tomography; PTH, parathyroid hormone; PINP, intact pro-collagen type I N-terminal pro-peptide; TMV, Turnover, mineralization, and volume; TRAP5b, tartrate resistant acid phosphatase type 5b; μCT, micro computed tomography.

* Corresponding author at: Division of Nephrology, University Hospitals Leuven, Herestraat 49, B-3000 Leuven, Belgium.
E-mail address: Pieter.Evenepoel@uzleuven.be (P. Evenepoel).

https://doi.org/10.1016/j.bonr.2022.101172
Received 19 January 2022; Accepted 3 February 2022
Available online 7 February 2022

strength, which are not captured by DXA (Ketteler et al., 2018). Further, DXA does not allow for a distinction between cortical and trabecular bone compartments. Glucocorticoids, still a mainstay in most immunosuppressive protocols, predominantly cause trabecular bone loss (Chotiyarnwong and McCloskey, 2020), while excessive PTH signaling triggers loss of cortical bone (Malluche et al., 2018), resulting in decreased cortical density and increased cortical porosity and thinning (Nickolas et al., 2013). This differential effect on bone compartments may explain why patients with chronic kidney disease (CKD) mainly sustain fractures at the peripheral, cortical-rich bone sites (Bjørnerem, 2016; Naylor et al., 2013).

Bone micro-architecture can be assessed *in vivo* by imaging techniques (high-resolution peripheral quantitative computed tomography; HRpQCT) (Nishiyama et al., 2015) or *ex vivo* by quantitative histomorphometry (Carvalho et al., 2016) or micro computed tomography (μCT) (Sharma et al., 2018) of bone biopsies. The maximum resolution of HRpQCT is 80 μm, limiting the evaluation of cortical porosity. μCT, on the other hand, achieves resolutions down to 5 μm, which allows quantification of cortical three-dimensional (3D) parameters in *ex vivo* samples (Akhter and Recker, 2020).

The primary aim of the present study was to investigate the impact of kidney transplantation on bone microarchitecture. Secondary aims included identifying determinants of cortical bone microarchitecture at 12 months post kidney transplantation.

2. Materials and methods

2.1. Study population

This is a subgroup-analysis of a prospective, observational study on the evolution of mineral and bone disorders after kidney transplantation (clinical trial identifier: NCT01886950). Patients referred for a single kidney transplantation at the University Hospitals Leuven between October 2010 and March 2016 were included. For the current study, patients with paired, research-protocolled iliac crest bone biopsies at the time of transplantation and 1 year later were included ($n = 30$). Demographic variables, including details of medical therapy, were retrieved from electronic files.

2.2. Biochemical analysis

Non-fasting blood samples were collected at both time-points. Creatinine, hemoglobin, total calcium, phosphate, and total alkaline phosphatase (total ALP) were measured by standard laboratory techniques. Albumin was measured by the bromocresol green method. Serum 1.25-OH_2 vitamin D (calcitriol) and 25-OH vitamin D (calcidiol) levels (Bouillon et al., 1984; Bouillon et al., 1980), as well as full-length (biointact) PTH (Bouillon et al., 1990) were determined by immunoradiometric assays. The estimated glomerular filtration rate (eGFR) was calculated using the Chronic Kidney Disease Epidemiology Collaboration (CKD-EPI) equation (Inker et al., 2012). Bone-specific alkaline phosphatase (BALP), whole (intact) pro-collagen type I N-terminal propeptide (PINP) and tartrate resistant acid phosphatase type 5b (TRAP5b) were measured with the IDS iSYS instrument (Immunodiagnostic Systems, Boldon, UK). Normal values are 6.1–23.9 μg/L for BALP, 12.8–82.6 ng/mL for PINP, and 1.1–6.9 U/L for TRAP5b, as given by the manufacturer. For all assays, the coefficients of variation were below 10%.

2.3. Immunosuppressive therapy

Standard triple immunosuppressive therapy with glucocorticoids, mycophenolate mofetil, and a calcineurin inhibitor (tacrolimus or cyclosporine) were initiated at time of transplantation. Intravenous methylprednisolone was given on the day of transplantation (500 mg), with an additional dose on the first post-operative day (40 mg). Oral prednisolone was then initiated at 16 mg/day, and tapered to 8 mg/day during the second, and 4 mg/day during the third month. Clinical parameters and results of a protocolled kidney graft biopsy decided whether steroids were halted or continued at a low dose from three months post-transplantation. Tacrolimus-dosing was controlled based on trough-levels, and mycophenolate mofetil was adjusted in cases of intolerance.

2.4. Bone sample retrieval and processing

Iliac crest bone biopsies were performed under general anesthesia in the operating room (baseline) or under light sedation with midazolam as an outpatient procedure (follow-up). Samples were extracted from a point 2 cm posterior and 2 cm inferior to the anterior iliac spine, by a horizontal approach, using a trephine with a 4.50/3.55 mm outer/inner diameter (Biopsybell 8G, Mirandola, Italy). Prior to follow-up at 12 months post-transplantation, patients received oral tetracycline twice (2×500 mg/day for 2 days), separated by an 11-day tetracycline-free interval. Bone biopsies were performed four days after the last intake of tetracycline. Due to the unpredictable timing of deceased donor transplantation, no tetracycline labeling was performed prior to baseline samples.

For each patient, two bone samples were retrieved; one sample for molecular diagnostics, collected in AllProtect Tissue Reagent (Qiagen, Hilden, Germany) and a separate sample for bone histomorphometry, which was fixed in 70% ethanol and embedded in a methylmethacrylate (MMA)-based resin. Un-decalcified 5 μm thick sections were stained by the Goldner method for determination of static bone parameters, while 10 μm thick unstained sections were mounted in 100% glycerol for fluorescence microscopy to visualize tetracycline labels and determine the dynamic parameters. All bone histomorphometric parameters are reported in two dimensions (2D) using standardized nomenclature (Dempster et al., 2013).

2.5. Bone histomorphometric analysis

The turnover, mineralization, and volume (TMV) classification was based on a semi-quantitative analysis by an experienced bone pathologist, taking into account key dynamic and static parameters using reference ranges as previously published (Salusky et al., 1988; Behets et al., 2015). Bone turnover was evaluated by the bone formation rate per total tissue area (normal range 97–613 um^2/mm^2/day). In the absence of tetracycline labeling, cutoffs of static histomorphometry previously published (Jørgensen et al., 2021a) was used to evaluate bone turnover, based on the following cutoffs: osteoblast perimeter per bone perimeter (1.88–5.37%), osteclast perimeter per bone perimeter (0.89–1.46%), osteoid area per bone area (1.63–2.44%) – and the presence or absence of fibrosis. Bone mineralization was considered delayed if osteoid area per bone area was >5% with prolonger mineralization lag time (>50 days), or, in cases without tetracycline labeling, if osteoid area per bone area >5% without high bone turnover. Bone volume was considered low when bone area per total tissue area (%) was <16.8%. Cortical bone analysis was performed using an image analysis program (AxioVision version 4.51, Zeiss Microscopy, Zeiss, Germany) running a custom program to calculate porosity values.

2.6. Micro-CT analysis

Paired bone biopsy samples stored in AllProtect at baseline and follow-up were scanned to evaluate longitudinal changes in bone microarchitecture. In addition, MMA embedded bone cores at follow-up were scanned to enable between-method comparison of μCT *vs* histomorphometric parameters. Whole biopsy cores were scanned using Skyscan Model 1172 μCT scanner (Bruker, Aartselaar, Belgium) at 50 kV, 200 mA with a 0.5-mm aluminum filter using an isotropic voxel size of 11 μm. Average exposure time was 1180 milliseconds. Images were

captured every 0.4° through 180° and then reconstructed using NRecon software (version 1.7.1.0, Bruker, Belgium). The average scan time was 60 min per sample. Analysis of bone samples was performed with CTAn software (version 1.16.4.1, Bruker, Belgium). The cortical region of interest (ROI) was independently defined in baseline and follow-up scans. Segmentation of the external cortical envelope was done by manual contouring every 25 slices, with interpolated ROIs for the in-between slices, and trabecular bone was defined beginning 5 mm after the border of cortical bone, to avoid including the transitional region. This was followed by application a global threshold interval of 85–255 Hounsfield units to isolate mineralized bone from un-mineralized sections based on histogram analysis. This dataset was further processed with a de-speckle operation to remove small isolated noise elements of 5 voxels or less, followed by 3D analysis to assess bone volume by tissue volume (BV/TV, %), microarchitecture parameters such as trabecular thickness (μm), number (mm^{-1}) and separation (μm), cortical thickness (μm) and porosity (%). Cortical porosity was defined as the sum of open and closed pores, and cortical thickness was measured as the width of the region of interest located at the mid-length of the external cortical section.

2.7. Statistical analysis

Descriptive statistics are reported as mean ± standard deviation (SD) or median [interquartile range, IQR] according to variable distribution. Paired Student's *t*-test or Wilcoxon matched-pairs signed-rank test were used to evaluate differences between baseline and follow-up parameters. Associations between continuous variables were evaluated by Spearman's rank correlation. XY- and Bland-Altman plots were drawn to compare data from μCT *vs* histomorphometry and visualize any systematic bias. For all analyses, a two-sided $p < 0.05$ was considered statistically significant.

3. Results

3.1. Characteristics of the study population

Mean age at time of transplantation was 57 ± 10 years, 73% ($n = 22$) were men, and 20% ($n = 6$) had diabetes. Twenty (67%) patients received chronic intermittent hemodialysis prior to transplantation, nine (30%) received continuous peritoneal dialysis, and a single patient was transplanted pre-emptively. Median dialysis vintage was 19 [IQR 9 to 29] months. The cause of CKD was glomerulonephritis/vasculitis in 7 (23%), cystic/hereditary/congenital in 6 (20%), hypertension/large vessel disease in 5 (17%), diabetic nephropathy in 4 (13%), other in 2 (7%), and unknown in 6 (20%). Two patients (6%) had previously undergone a parathyroidectomy.

At 1-year post-transplantation, mean eGFR was 48 ± 19 mL/min/1.73 m^2, with a range from 19 to 106 mL/min/1.73 m^2. Three patients (10%) had an eGFR <30 and none <15 mL/min/1.73 m^2. Seventeen patients (57%) received cholecalciferol, 5 (17%) received active vitamin D, and 10 (33%) received calcium-supplements; none received calcimimetics or bisphosphonates. Six patients (20%) suffered at least one episode of acute rejection in the first post-transplantation year. Four patients (13%) had halted prednisolone by 12 months post-transplantation, and the median cumulative dose of steroid for all patients was 2.6 [IQR 1.9 to 2.9] g.

3.2. Longitudinal changes in kidney function and biochemistry

Biochemical measurements at time of and 12 months after kidney transplantation are shown in Table 1. As expected, levels of biointact PTH and phosphate decreased significantly, while total calcium levels increased slightly. Of the biochemical bone turnover markers, intact PINP decreased by 67%, TRAP5b by 52%, and total ALP by 29%, with a smaller, non-significant decrease for BALP (17%). At 1-year post-transplantation, 20 patients (67%) had persistent hyperparathyroidism (arbitrarily defined as biointact PTH >1.5 UNL), 7 (23%) had hypercalcemia (total calcium >10.3 mg/dL), 6 patients (20%) had hypophosphatemia (phosphate <2.3 mg/dL), and 2 patients (7%) had calcidiol levels <15 ng/mL.

Table 1
Biochemical variables at time of and 12 months after kidney transplantation.

	Transplantation ($n = 30$)	12 months post-transplantation ($n = 30$)	p
Albumin, g/L	43.2 ± 3.6	43.3 ± 4.0	0.98
Urea, mg/dL	106.3 ± 38.1	70.8 ± 29.6	<0.001
Creatinine, mg/dL	7.69 ± 2.54	1.64 ± 0.47	<0.001
Total calcium, mg/dL	9.60 ± 0.54	9.86 ± 0.73	0.04
Phosphate, mg/dL	4.85 ± 1.26	3.04 ± 0.75	<0.001
25-OH-vitamin D, μg/mL	47 ± 20	38 ± 12	0.04
Magnesium, mg/dL	2.25 ± 0.37	1.70 ± 0.21	<0.001
Biointact PTH, ρg/mL	273 [132; 441]	85 [47; 134]	<0.001
Biointact PTH, xUNL	6.8 [3.3; 11.0]	2.1 [1.2; 3.3]	
Alkaline phosphatase, U/L	94 [78; 139]	82 [67; 96]	0.02
BALP, μg/mL	29.6 [15.1; 44.2]	24.3 [17.8; 32.9]	0.31
Intact PINP, μg/mL	109 [61; 196]	60 [35; 106]	0.04
TRAP5b, U/L	6.21 [3.94; 9.13]	3.88 [3.12; 5.01]	0.003

Data are mean ± SD or median [IQR], with p by paired Student's *t*-test; skewed variables converted to their natural logarithm for parametric testing.
Abbr.: BALP = bone-specific alkaline phosphatase, PINP = pro-collagen type I N-terminal pro-peptide, PTH = parathyroid hormone, xUNL = times upper normal limit, TRAP5b = tartrate resistant acid phosphatase type 5b.

3.3. Longitudinal changes in bone turnover, mineralization, volume, and microarchitecture

Bone histomorphometry showed significant reductions in eroded perimeters and the presence of marrow fibrosis (Table 2). The number of patients with high turnover bone disease decreased from 19 to 0% ($p < 0.001$). At 12-months post-transplantation, bone turnover was low in 5 (17%) and normal in 25 (83%) patients – delayed mineralization was seen in 5 (17%) and low bone volume in 8 (27%) patients. By μCT, there was a small, significant decrease in trabecular thickness after kidney transplantation, with a non-significant reduction in trabecular bone volume (Table 2). The remaining parameters of cortical and trabecular bone microarchitecture were overall unchanged 12 months after kidney transplantation, albeit with substantial inter-individual variation (Fig. 1A and B).

Similarly, no overall changes were seen for DXA-derived BMD at spine and hip, but the range of variation in the percentage change per year was substantial (Fig. 2).

Table 3 shows bone microarchitecture for different categories of the TMV classification at 1-year post-transplantation. Patients with low bone turnover had lower trabecular bone volume, with lower trabecular number and higher trabecular separation by μCT compared to patients with normal bone turnover.

3.4. Predictors of post-transplantation μCT bone volume and microarchitecture

Older age was associated with lower trabecular bone volume (*rho* − 0.56, $p = 0.002$), lower trabecular number (*rho* − 0.65, $p < 0.001$), and higher trabecular separation (*rho* = 0.48, $p = 0.01$). Gender, body mass index, diabetes, and dialysis vintage were not associated with μCT bone volume or microarchitecture at 12 months.

No significant correlations were found between biointact PTH-levels

Table 2
Changes in bone by micro computed tomography, histomorphometry, and dual-energy x-ray absorptiometry from baseline to 12 months post-transplantation.

	Baseline (n = 30)	12 months (n = 30)	p
Micro CT			
Trabecular bone volume/tissue volume, %	17.3 ± 5.1	15.3 ± 5.5	0.08
Trabecular thickness, μm	134.2 ± 18.7	124.9 ± 12.7	0.003
Trabecular separation, μm	659 ± 132	674 ± 133	0.59
Trabecular number, mm^{-1}	1.30 ± 0.42	1.23 ± 0.46	0.48
Cortical porosity, %	10.2 [7.9; 16.3]	9.5 [7.3; 14.6]	0.15
Cortical thickness, μm	729.3 ± 247.8	712.5 ± 268.6	0.73
Histomorphometry			
Turnover			
Low/normal/high, %	22/59/19%	17/83/0%	0.001
Bone formation rate/total tissue area, $\mu m^2/mm^2$/day.	N/A	153 [76, 285]	–
Osteoblast perimeter/bone perimeter, %	3.8 [0.0; 9.5]	5.7 [2.5; 10.8]	0.17
Osteoclast perimeter/bone perimeter, %	0.6 [0.0; 1.5]	0.5 [0.3; 1.2]	0.99
Eroded perimeter/bone perimeter, %	4.0 [2.4; 5.1]	2.1 [1.2; 3.5]	0.01
Fibrosis, yes	41%	0%	<0.001
Mineralization			
Delayed/normal, %	0/100%	17/83%	0.03
Mineralization lag time, days	N/A	35 [20, 65]	–
Osteoid area/bone area, %	2.0 [1.3; 3.9]	3.3 [1.2; 5.4]	0.32
Osteoid perimeter/bone perimeter, %	18.9 [14.3; 26.7]	24.8 [13.1; 38.4]	0.15
Volume			
Low/normal, %	37/63%	27/73%	0.87
Bone area/total tissue area, %	19.3 ± 7.0	19.7 ± 5.6	0.52
Trabecular thickness, μm	132.1 ± 35.3	128.8 ± 30.3	0.82
Trabecular separation, μm	446 ± 181	406 ± 120	0.10
Trabecular number, mm^{-1}	1.87 ± 0.50	1.96 ± 0.46	0.20
Cortical porosity, %	7.4 [5.2; 9.5]	8.2 [4.7; 14.7]	0.41
Dual energy x-ray absorptiometry (n = 16)			
Lumbar spine BMD, g/cm^2	0.873 ± 0.118	0.894 ± 0.113	0.48
Lumbar spine T-score	−2.37 ± 0.97	−2.30 ± 0.71	0.40
Lumbar spine Z-score	−1.77 ± 0.99	−1.75 ± 0.76	0.53
Femoral neck BMD, g/cm^2	0.615 ± 0.103	0.606 ± 0.107	0.43
Femoral neck T-score	−2.42 ± 0.80	−2.50 ± 0.89	0.59
Femoral neck Z-score	−1.50 ± 0.75	−1.64 ± 0.75	0.71

Data are mean(SD), median[IQI], or %, with p by paired Student's t-test, Wilcoxon matched-pairs signed-rank test, or Pearson's X^2 test, respectively.

at 12 months post-transplantation and bone microarchitecture. Total ALP was directly correlated to higher cortical porosity (*rho* 0.45, p = 0.01) as was BALP (*rho* 0.44, p = 0.02), while this was not the case for intact PINP (*rho* 0.20, p = 0.29), or TRAP5b (*rho* 0.20, p = 0.29). Total ALP was also inversely correlated to cortical thickness (*rho* − 0.45, p = 0.01).

3.5. Predictors of changes in μCT bone volume and microarchitecture

There was a trend towards greater increase in cortical porosity for women (2.4% *vs.* −2.5%, p = 0.05), and patients with diabetes (3.0% *vs.* −2.2%, p = 0.07) during the first post-transplantation year. Age, dialysis vintage, and cumulative steroid dose were unrelated to changes in bone microarchitecture by μCT (data not shown). Changes in biointact PTH and bone turnover markers (BALP, intact PINP, TRAP5b) were also unrelated to changes in μCT parameters of cortical and trabecular bone microarchitecture (Supplementary Table 1).

3.6. Agreement between μCT and histomorphometry

To evaluate the agreement between μCT and histomorphometry, we compared bone volume and microarchitecture parameters at baseline, using μCT scans of the MMA-embedded bone-cores at follow-up (n = 27). Spearman's correlation coefficients were as follows: cortical porosity (*rho* 0.509, p = 0.007), bone volume/tissue volume (*rho* 0.593, p = 0.001), trabecular thickness (*rho* 0.545, p = 0.005), trabecular separation (*rho* 0.336, p = 0.10), and trabecular number (*rho* 0.379, p = 0.06). XY- and Bland-Altman plots are shown in Fig. 3. No obvious bias could be detected for trabecular parameters, while for cortical porosity, μCT-measurements were systematically higher than by histomorphometry.

4. Discussion

The main finding of this study is that contemporary kidney transplantation has a minimal impact on trabecular and cortical bone microarchitecture. Further, the assessment of bone microarchitecture by histomorphometry and μCT show only moderate agreement.

By the bone histomorphometric analysis, modest changes were seen 12 months following kidney transplantation, with reduced bone resorption and the disappearance of disordered bone formation (fibrosis). These findings are in concordance with other contemporary studies evaluating post-transplantation bone disease using bone histomorphometry as the standard (Marques et al., 2017; Keronen et al., 2019).

By μCT, a small reduction in trabecular thickness was detected, but trabecular bone volume was overall unchanged at 12 months. While earlier studies reported substantial bone loss in the first year post-transplantation (Julian et al., 1991; Heaf, 2003), stability of trabecular bone mass is a consistent finding in contemporary kidney transplant recipients (Iyer et al., 2014; Evenepoel et al., 2020; Evenepoel et al., 2017; Marques et al., 2019). As several studies demonstrated a relationship between cumulative steroid dose and post-transplantation bone loss (Evenepoel et al., 2017; Monier-Faugere et al., 2000; Parker et al., 1999; Rojas et al., 2003), the introduction of steroid minimization protocols has been proposed as an explanation for this beneficial trend (Iyer et al., 2014; Kidney Disease: Improving Global Outcomes (KDIGO) CKD-MBD Update Work Group, 2017).

The cortical parameters of porosity and thickness were overall unchanged 1-year after kidney transplantation. Both improvement and deterioration of bone microarchitecture has previously been reported in the early post-transplant period (Iyer et al., 2014; Marques et al., 2019). Iyer et al. described significant cortical bone loss, with reductions in cortical area, thickness, and density at the distal radius and tibia as evaluated by HRpQCT in a cohort of kidney transplant recipients (Iyer et al., 2014). In contrast, improved cortical parameters were reported by Marques et al. by bone histomorphometry performed at time of and 1-year post kidney transplantation (Marques et al., 2019). It is worth noting that in the study by Iyer et al., bone turnover markers *increased* post-transplantation, indicating an overall increase in skeletal remodeling rate, and the detriments in cortical micro-architecture paralleled the severity of hyperparathyroidism (Iyer et al., 2014). We speculate that withdrawal of bone modulating therapy, such as calcimimetics, at time of transplantation might have contributed to increased bone turnover post-transplantation (Evenepoel et al., 2012). In the study by Marquest et al., PTH and bone turnover markers *decreased* during the first post-transplant year (Marques et al., 2019), similar to what we find in the present cohort. In our study, we did not find the expected relationship between cortical parameters and biointact PTH levels; neither were there any clear association between the changes in biointact PTH and the changes in bone microarchitecture. Higher levels of BALP associated with greater cortical porosity at 12-months post-transplantation, which could indicate a detrimental effect of high turnover bone disease. Thus, we hypothesize that a tighter control of

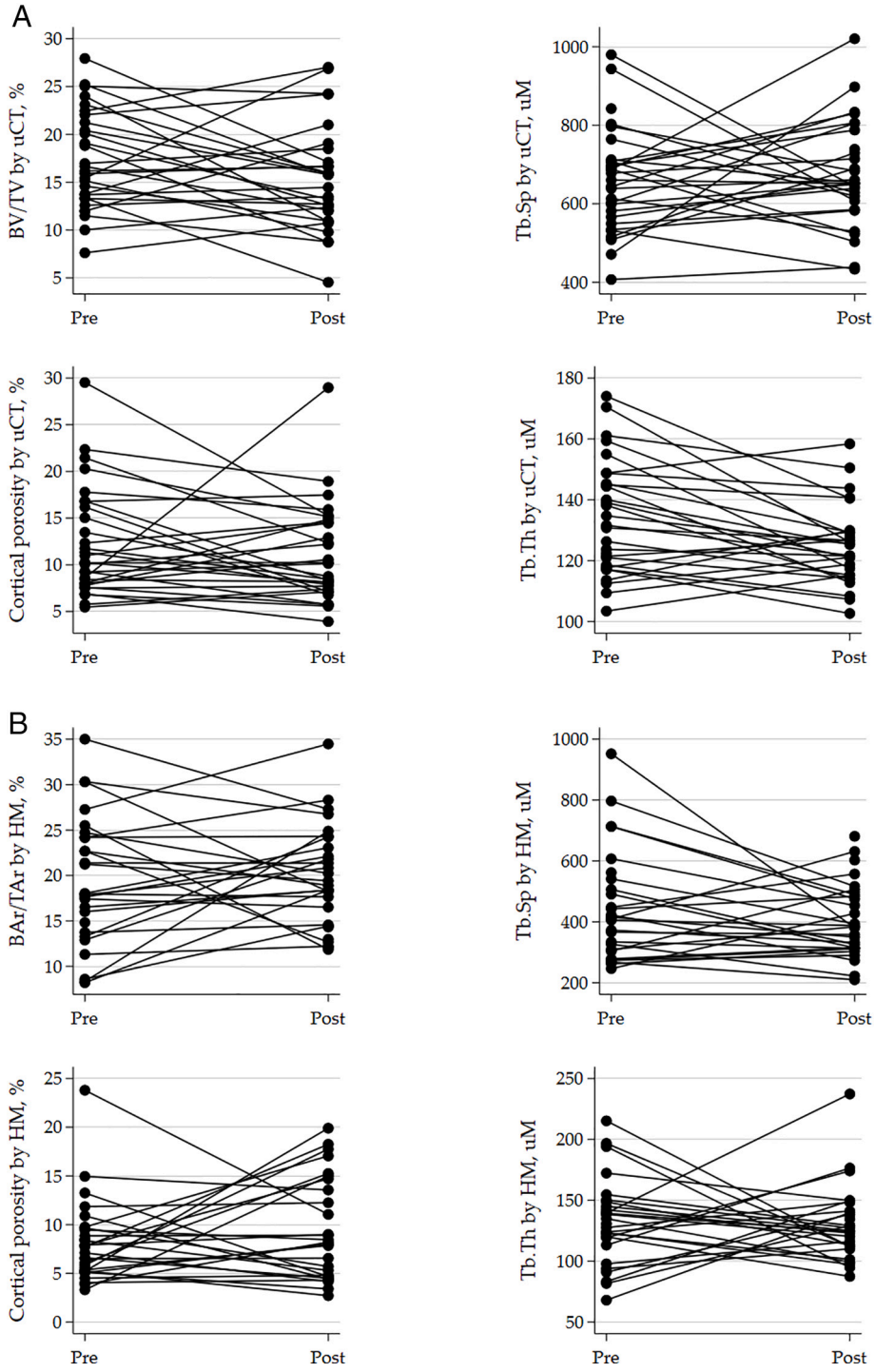

Fig. 1. A Changes in bone volume and micro-architecture by μCT from time of to 1-year post kidney transplantation.
B Changes in bone area and micro-architecture by histomorphometry from time of to 1-year post kidney transplantation.

hyperparathyroidism pre-transplantation, and normalization of bone turnover post-transplantation, may explain the limited changes in cortical bone microarchitecture seen in the current cohort.

Comparing complementary variables of μCT and histomorphometry, correlations were moderately good for bone volume and cortical porosity, but rather poor for trabecular microarchitecture. These findings are in line with what was demonstrated in two previous studies, one including healthy adults, postmenopausal women, and patients with renal osteodystrophy (Tamminen et al., 2011), and the other investigating bone health in children with CKD (Pereira et al., 2016). Both of these studies reported moderate correlation coefficients in the range of 0.39–0.71. Notably higher correlation coefficients were demonstrated by Recker et al. in healthy, elderly men (0.76–0.86) (Recker et al., 2018). Such a discrepancy could be related to the mineralization defects seen in CKD, as osteoid is not visualized in the μCT images. The first post-transplant year is a highly dynamic time-period, with marked changes in skeletal remodeling rate following the resolution of secondary hyperparathyroidism. Increased amounts of osteoid, interpreted as delayed bone mineralization, has been demonstrated at 1 year post-transplant (Jørgensen et al., 2021b), which could contribute to weakening the

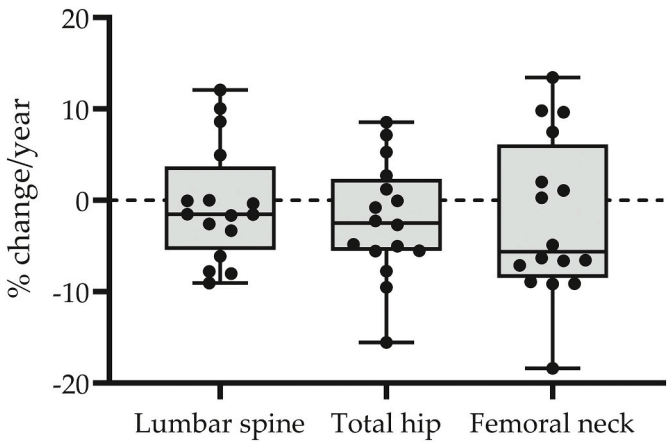

Fig. 2. Change in bone mineral density (BMD, %/year) at lumbar spine, total hip, and femoral neck by dual-energy x-ray absorptiometry from time of to 1-year post kidney transplantation.

correlations between μCT and histomorphometric measurements. Disparities between the 2D and 3D versions of the same μCT-variables has also been demonstrated (Chappard et al., 2005), highlighting the challenge of comparing the 2D structures of bone biopsy sections to 3D structural models and imaging.

Other potential sources of variability include inter- and intra-observer, as well as between- and within-sample variability. In the present study, μCT and bone histomorphometric analyses were both performed by a single observer, thereby eliminating inter-observer variability. Intra-observer variability is substantial for bone histomorphometry (5–15%) (Pødenphant et al., 1986), but has been shown to be considerably lower (1.3–3.2%) for repeated μCT analyses (Chappard et al., 2008). For the correlation analyses between histomorphometry and μCT, we used μCT scans of the MMA-embedded bone-cores to eliminate sample site variability, which was previously shown to be as high as 30%, when comparing bone histomorphometry of samples from the left and right hip (Parisien et al., 1988). Within-sample variability has been evaluated for μCT by comparing scans of different sections from the same bone core, with CVs for the different parameters ranging from 1.8 to 7.1% (Chappard et al., 2008). All these sources of variability may have contributed to the moderate correlations reported here. Lastly, image analysis settings, such as ROI selection and the thresholds applied might contribute to differences between the two analytical techniques.

4.1. Strengths and limitations

Strengths of this study include the longitudinal design and the completeness of data available for bone phenotyping. Bone biopsies were part of a research protocol, and thus, results should not be biased by indication. Limitations include the small sample size, which, together with the inherent measurement variability discussed above, may have limited our ability to detect discrete changes in bone microarchitecture. The duration of follow-up was also relatively short, considering the slow metabolism of skeletal tissue. Despite these limitations, this is one of the few studies evaluating bone microarchitecture longitudinally using both μCT and histomorphometry, and the largest cohort so far to investigate micro-architectural changes in kidney transplant recipients.

4.2. Conclusions

In conclusion, contemporary kidney transplantation has a limited impact on bone microarchitecture. This beneficial outcome may be a reflection of normalization of skeletal remodeling due to the resolution of secondary hyperparathyroidism post-transplantation.

Supplementary data to this article can be found online at https://doi.org/10.1016/j.bonr.2022.101172.

Funding sources

HSJ was supported by a European Renal Association (ERA) long-term fellowship during the completion of this work. This research did not receive further specific grants from funding agencies in the public, commercial, or not-for-profit sectors.

CRediT authorship contribution statement

Conceptualization: PE, PDH; Data curation: HL; Formal analysis: CM, HJ; Investigation: PE, HL, CM; Project administration: PE; Resources:

Table 3
Bone volume, microarchitecture and density in categories of bone turnover, mineralization, and volume at 12 months after kidney transplantation.

	Turnover		Mineralization		Volume	
	Low ($n = 5$)	Normal ($n = 25$)	Delayed ($n = 5$)	Normal ($n = 25$)	Low ($n = 8$)	Normal ($n = 22$)
Micro computed tomography						
Bone volume/tissue volume, %	10.1 ± 4.3	16.3 ± 5.1 †	15.8 ± 5.7	15.2 ± 5.6	12.8 ± 2.6	16.2 ± 6.1
Trabecular thickness, μm	127.10 ± 18.69	124.39 ± 11.59	123.63 ± 7.50	125.06 ± 13.45	136.24 ± 14.17	120.16 ± 8.90 †
Trabecular separation, μm	778.8 ± 152.5	651.8 ± 120.3 †	674.5 ± 123.9	673.6 ± 136.4	713.5 ± 60.1	652.8 ± 145.8
Trabecular number, mm^{-1}	0.77 ± 0.25	1.33 ± 0.44 †	1.28 ± 0.42	1.22 ± 0.48	0.94 ± 0.17	1.34 ± 0.49 †
Cortical thickness, μm	842 ± 269	687 ± 266	658 ± 219	723 ± 280	563 ± 71	763 ± 300*
Cortical porosity, %	7.4 [5.5; 14.8]	10.1 [7.8; 14.7]	17.5 [9.2; 24.0]	8.5 [7.1; 13.7] †	8.3 [7.5; 13.4]	10.6 [7.4; 14.9]
Histomorphometry						
Bone area/Tissue area, %	18.18 ± 6.14	19.99 ± 5.54	20.46 ± 6.85	19.51 ± 5.43	13.14 ± 1.13	22.17 ± 4.41 †
Trabecular thickness, μm	133.40 ± 15.03	127.78 ± 32.72	119.80 ± 20.23	130.61 ± 31.99	110.02 ± 15.34	135.88 ± 31.72 †
Trabecular separation, μm	486.0 ± 171.8	389.7 ± 104.3	367.9 ± 123.3	414.3 ± 121.0	549.1 ± 77.8	351.8 ± 83.2 †
Trabecular number, mm^{-1}	1.71 ± 0.46	2.02 ± 0.45	2.14 ± 0.50	1.93 ± 0.45	1.54 ± 0.20	2.13 ± 0.42 †
Cortical porosity, %	8.0 [3.0; 14.3]	8.3 [4.8; 14.8]	8.1 [4.6; 15.1]	8.4 [6.1; 11.2]	8.2 [4.7; 14.7]	8.4 [4.4; 15.0]
Dual energy x-ray absorptiometry ($n = 16$)						
Lumbar spine BMD, g/cm^2	0.856 ± 0.129	0.900 ± 0.113	0.904 ± 0.077	0.892 ± 0.119	0.850 ± 0.064	0.914 ± 0.126
Lumbar spine *T*-score	−2.37 ± 1.66	−2.29 ± 0.60	−1.92 ± 0.70	−2.40 ± 0.71	−2.41 ± 0.58	−2.22 ± 0.84
Lumbar spine *Z*-score	−1.74 ± 1.51	−1.75 ± 0.70	−1.28 ± 0.59	−1.87 ± 0.77	−1.76 ± 0.59	−1.74 ± 0.93
Femoral neck BMD, g/cm^2	0.596 ± 0.141	0.608 ± 0.106	0.621 ± 0.071	0.604 ± 0.113	0.574 ± 0.153	0.622 ± 0.080
Femoral neck *T*-score	−2.66 ± 1.38	−2.48 ± 0.88	−2.27 ± 0.52	−2.56 ± 0.97	−2.62 ± 1.13	−2.40 ± 0.70
Femoral neck *Z*-score	−1.71 ± 1.24	−1.63 ± 0.72	−1.33 ± 0.43	−1.72 ± 0.80	−1.66 ± 0.92	−1.63 ± 0.63

Data are mean ± SD or median [IQR], with † = $p < 0.05$ and * = $p < 0.10$ by Student's *t*-test or Wilcoxon rank-sum test, respectively.
Abbr.: BMD = bone mineral density.

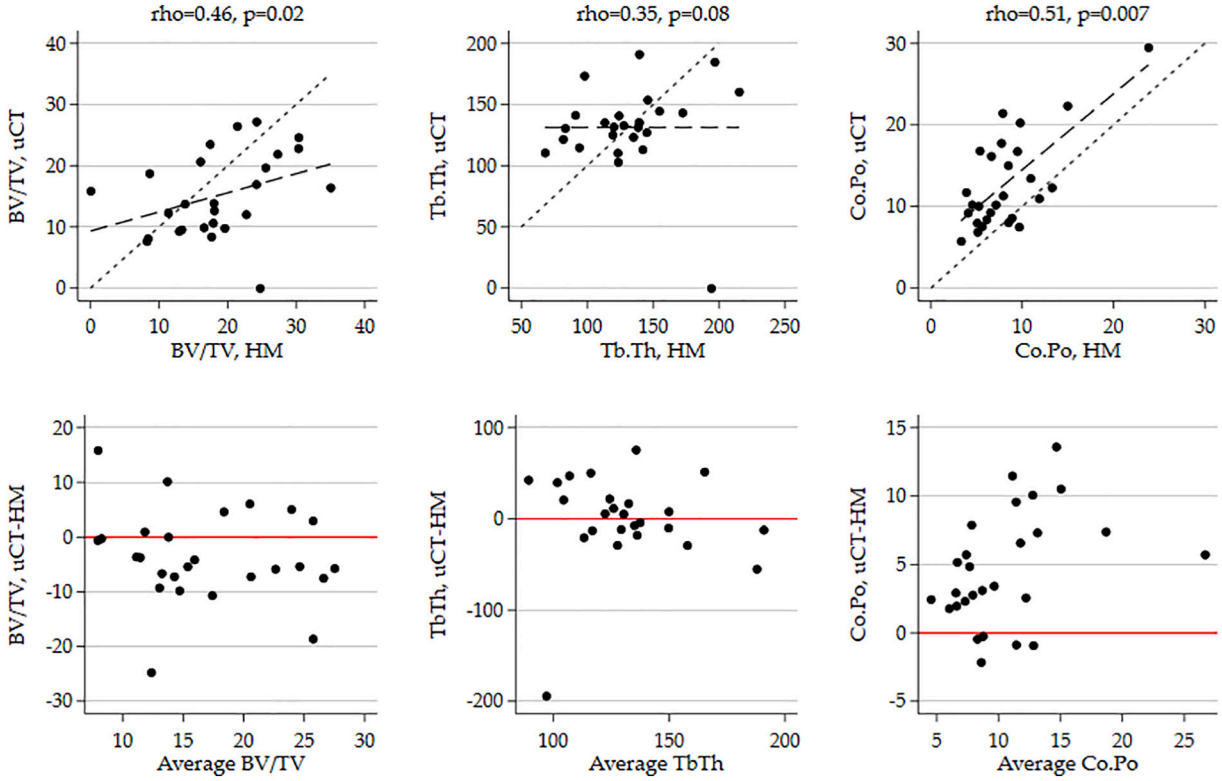

Fig. 3. XY- and Bland-Altman plots for the agreement between parameters of bone volume and micro-architecture by micro CT (μCT) *versus* histomorphometry (HM), BV/TV = bone volume/tissue volume, TbTh = trabecular thickness, CoPo = cortical porosity, rho = Spearman's correlation coefficient.

PE, PDH; Supervision: PE; Visualization: CM, HJ; Writing - original draft: CM, HJ; Writing - review & editing: CM, HJ, LV, NB, HL, PDH, GC, PE.

Declaration of competing interest

PE reports personal fees from Amgen and Vifor-FMC. Remaining authors have no conflicts of interest to declare.

Acknowledgements

HSJ was supported by a European Renal Association (ERA) long-term fellowship during the completion of this work. The authors would like to acknowledge G. Behets for performing the bone histomorphometric analyses, and M. Dekens and J. Paulissen of the Nephrology and Renal Transplantation Research Group for their excellent assistance with laboratory work and μCT image aquisition.

References

Akhter, M.P., Recker, R.R., 2020. High resolution imaging in bone tissue research-review. Bone, 115620. https://doi.org/10.1016/j.bone.2020.115620. Published online August.

Ball, A.M., Gillen, D.L., Sherrard, D., et al., 2002. Risk of hip fracture among dialysis and renal transplant recipients. JAMA 288 (23), 3014–3018. https://doi.org/10.1001/jama.288.23.3014.

Behets, G.J., Spasovski, G., Sterling, L.R., et al., 2015. Bone histomorphometry before and after long-term treatment with cinacalcet in dialysis patients with secondary hyperparathyroidism. Kidney Int. 87 (4), 846–856. https://doi.org/10.1038/ki.2014.349.

Bjørnerem, Å., 2016. The clinical contribution of cortical porosity to fragility fractures. Bonekey Rep. 5, 846. https://doi.org/10.1038/bonekey.2016.77.

Bouillon, R., De Moor, P., Baggiolini, E.G., Uskokovic, M.R., 1980. A radioimmunoassay for 1,25-dihydroxycholecalciferol. Clin. Chem. 26 (5), 562–567. http://www.ncbi.nlm.nih.gov/pubmed/6894888.

Bouillon, R., Van Herck, E., Jans, I., Tan, B.K., Van Baelen, H., De Moor, P., 1984. Two direct (nonchromatographic) assays for 25-hydroxyvitamin D. Clin. Chem. 30 (11), 1731–1736.

Bouillon, R., Coopmans, W., Degroote, D.E., Radoux, D., Eliard, P.H., 1990. Immunoradiometric assay of parathyrin with polyclonal and monoclonal region-specific antibodies. Clin. Chem. 36 (2), 271–276.

Bouquegneau, A., Salam, S., Delanaye, P., Eastell, R., Khwaja, A., 2016. Bone disease after kidney transplantation. Clin. J. Am. Soc. Nephrol. 11 (7), 1282–1296. https://doi.org/10.2215/CJN.11371015.

Carvalho, C., Magalhães, J., Pereira, L., Simóes-Silva, L., Castro-Ferreira, I., Frazão, J.M., 2016. Evolution of bone disease after kidney transplantation: a prospective histomorphometric analysis of trabecular and cortical bone. Nephrology 21 (1), 55–61. https://doi.org/10.1111/nep.12570.

Chappard, D., Retailleau-Gaborit, N., Legrand, E., Baslé, M.F., Audran, M., 2005. Comparison insight bone measurements by histomorphometry and μCT. J. Bone Miner. Res. 20 (7), 1177–1184. https://doi.org/10.1359/JBMR.050205.

Chappard, C., Marchadier, A., Benhamou, L., 2008. Interindividual and intraspecimen variability of 3-D bone microarchitectural parameters in iliac crest biopsies imaged by conventional micro-computed tomography. J. Bone Miner. Metab. 26 (5), 506–513. https://doi.org/10.1007/s00774-008-0856-2.

Chotiyarnwong, P., McCloskey, E.V., 2020. Pathogenesis of glucocorticoid-induced osteoporosis and options for treatment. Nat. Rev. Endocrinol. 16 (8), 437–447. https://doi.org/10.1038/s41574-020-0341-0.

Dempster, D.W., Compston, J.E., Drezner, M.K., et al., 2013. Standardized nomenclature, symbols, and units for bone histomorphometry: a 2012 update of the report of the ASBMR histomorphometry nomenclature committee. J. Bone Miner. Res. 28 (1), 2–17. https://doi.org/10.1002/jbmr.1805.

Evenepoel, P., Sprangers, B., Lerut, E., et al., 2012. Mineral metabolism in renal transplant recipients discontinuing cinacalcet at the time of transplantation: a prospective observational study. Clin. Transpl. 26 (3), 393–402. https://doi.org/10.1111/j.1399-0012.2011.01524.x.

Evenepoel, P., Behets, G.J., Viaene, L., D'Haese, P.C., 2017. Bone histomorphometry in de novo renal transplant recipients indicates a further decline in bone resorption 1 year posttransplantation. Kidney Int. 91 (2), 469–476. https://doi.org/10.1016/j.kint.2016.10.008.

Evenepoel, P., Claes, K., Meijers, B., et al., 2019. Bone mineral density, bone turnover markers, and incident fractures in de novo kidney transplant recipients. Kidney Int. 95 (6), 1461–1470. https://doi.org/10.1016/j.kint.2018.12.024.

Evenepoel, P., Claes, K., Meijers, B., et al., 2020. Natural history of mineral metabolism, bone turnover and bone mineral density in de novo renal transplant recipients treated with a steroid minimization immunosuppressive protocol. Nephrol. Dial. Transplant. 35 (4), 697–705. https://doi.org/10.1093/ndt/gfy306.

Heaf, J.G., 2003. Bone disease after renal transplantation. Transplantation 75 (3), 315–325. https://doi.org/10.1097/01.TP.0000043926.74349.6D.

Inker, L.A., Schmid, C.H., Tighiouart, H., et al., 2012. Estimating glomerular filtration rate from serum creatinine and cystatin C. N. Engl. J. Med. 367 (1), 20–29. https://doi.org/10.1056/NEJMoa1114248.

Iyer, S.P., Nikkel, L.E., Nishiyama, K.K., et al., 2014. Kidney transplantation with early corticosteroid withdrawal: paradoxical effects at the central and peripheral skeleton. J. Am. Soc. Nephrol. 25 (6), 1331–1341. https://doi.org/10.1681/ASN.2013080851.

Jørgensen, H.S., Behets, G., Viaene, L., et al., 2021. Static histomorphometry allows for a diagnosis of bone turnover in renal osteodystrophy in the absence of tetracycline labels. Bone 152, 116066. https://doi.org/10.1016/j.bone.2021.116066.

Jørgensen, H.S., Behets, G., Bammens, B., et al., 2021. Patterns of renal osteodystrophy 1 year after kidney transplantation. Nephrol. Dial. Transplant. 36 (11), 2130–2139. https://doi.org/10.1093/ndt/gfab239.

Julian, B.A., Laskow, D.A., Dubovsky, J., Dubovsky, E.V., Curtis, J.J., Quarles, L.D., 1991. Rapid loss of vertebral mineral density after renal transplantation. N. Engl. J. Med. 325 (8), 544–550. https://doi.org/10.1056/NEJM199108223250804.

Keronen, S., Martola, L., Finne, P., Burton, I.S., Kröger, H., Honkanen, E., 2019. Changes in bone histomorphometry after kidney transplantation. Clin. J. Am. Soc. Nephrol. 14 (6), 894–903. https://doi.org/10.2215/CJN.09950818.

Ketteler, M., Block, G.A., Evenepoel, P., 2018. Diagnosis, evaluation, prevention, and treatment of chronic kidney disease-mineral and bone disorder: synopsis of the kidney disease: improving global outcomes 2017 clinical practice guideline update. Ann. Intern. Med. https://doi.org/10.7326/M17-2640. Published online February 20.

Kidney Disease: Improving Global Outcomes (KDIGO) CKD-MBD Update Work Group, 2017. KDIGO 2017 clinical practice guideline update for the diagnosis, evaluation, prevention, and treatment of chronic kidney disease–mineral and bone disorder (CKD-MBD). Kidney Int. Suppl. 7 (1), 1–59. https://doi.org/10.1016/j.kisu.2017.04.001.

Malluche, H.H., Monier-Faugere, M.C., Blomquist, G., Davenport, D.L., 2018. Two-year cortical and trabecular bone loss in CKD-5D: biochemical and clinical predictors. Osteoporos. Int. 29 (1), 125–134. https://doi.org/10.1007/s00198-017-4228-4.

Marques, I.D.B., Araújo, M.J.C.L.N., Graciolli, F.G., et al., 2017. Biopsy vs. Peripheral computed tomography to assess bone disease in CKD patients on dialysis: differences and similarities. Osteoporos. Int. 28 (5), 1675–1683. https://doi.org/10.1007/s00198-017-3956-9.

Marques, I.D.B., Araújo, M.J.C.L.N., Graciolli, F.G., et al., 2019. A randomized trial of zoledronic acid to prevent bone loss in the first year after kidney transplantation. J. Am. Soc. Nephrol. 30 (2), 355–365. https://doi.org/10.1681/ASN.2018060656.

Monier-Faugere, M.C., Mawad, H., Qi, Q., Friedler, R.M., Malluche, H.H., 2000. High prevalence of low bone turnover and occurrence of osteomalacia after kidney transplantation. J. Am. Soc. Nephrol. 11 (6), 1093–1099. https://doi.org/10.1681/ASN.V1161093.

Naylor, K.L., Li, A.H., Lam, N.N., Hodsman, A.B., Jamal, S.A., Garg, A.X., 2013. Fracture risk in kidney transplant recipients: a systematic review. Transplantation 95 (12), 1461–1470. https://doi.org/10.1097/TP.0b013e31828eead8.

Nickolas, T.L., Stein, E.M., Dworakowski, E., et al., 2013. Rapid cortical bone loss in patients with chronic kidney disease. J. Bone Miner. Res. 28 (8), 1811–1820. https://doi.org/10.1002/jbmr.1916 [doi].

Nishiyama, K.K., Pauchard, Y., Nikkel, L.E., et al., 2015. Longitudinal HR-pQCT and image registration detects endocortical bone loss in kidney transplantation patients. J. Bone Miner. Res. 30 (3), 554–561. https://doi.org/10.1002/jbmr.2358 [doi].

Parisien, M.V., McMahon, D., Pushparaj, N., Dempster, D.W., 1988. Trabecular architecture in iliac crest bone biopsies: infra-individual variability in structural parameters and changes with age. Bone 9 (5), 289–295. https://doi.org/10.1016/8756-3282(88)90012-9.

Parker, C.R., Freemont, A.J., Blackwell, P.J., Grainge, M.J., Hosking, D.J., 1999. Cross-sectional analysis of renal transplantation osteoporosis. J. Bone Miner. Res. 14 (11), 1943–1951. https://doi.org/10.1359/jbmr.1999.14.11.1943.

Pereira, R.C., Bischoff, D.S., Yamaguchi, D., Salusky, I.B., Wesseling-Perry, K., 2016. Micro-CT in the assessment of pediatric renal osteodystrophy by bone histomorphometry. Clin. J. Am. Soc. Nephrol. 11 (3), 481–487. https://doi.org/10.2215/CJN.04810515.

Pødenphant, J., Gotfredsen, A., Nilas, L., Nørgård, H., Braendstrup, O., Christiansen, C., 1986. Iliac crest biopsy: an investigation on certain aspects of precision and accuracy. Bone Miner. 1 (4), 279–287. http://www.ncbi.nlm.nih.gov/pubmed/3504710.

Recker, R.R., Akhter, M.K., Lappe, J.M., Watson, P., 2018. Bone histomorphometry in transiliac biopsies from 48 normal, healthy men. Bone 111, 109–115. https://doi.org/10.1016/j.bone.2018.03.019.

Rojas, E., Carlini, R.G., Clesca, P., et al., 2003. The pathogenesis of osteodystrophy after renal transplantation as detected by early alterations in bone remodeling. Kidney Int. 63 (5), 1915–1923. https://doi.org/10.1046/j.1523-1755.2003.00938.x.

Salusky, I.B., Coburn, J.W., Brill, J., et al., 1988. Bone diseae in pediatric patients undergoing dialysis with CAPD or CCPD. Kidney Int. 33 (5), 975–982. https://doi.org/10.1038/ki.1988.96.

Sharma, A.K., Toussaint, N.D., Masterson, R., et al., 2018. Deterioration of cortical bone microarchitecture: critical component of renal osteodystrophy evaluation. Am. J. Nephrol. 47 (6), 376–384. https://doi.org/10.1159/000489671.

Tamminen, I.S., Isaksson, H., Aula, A.S., Honkanen, E., Jurvelin, J.S., Kröger, H., 2011. Reproducibility and agreement of micro-CT and histomorphometry in human trabecular bone with different metabolic status. J. Bone Miner. Metab. 29 (4), 442–448. https://doi.org/10.1007/s00774-010-0236-6.